Wavefront propagation by the finite-difference method

The traveltimes of seismic wave propagation can be calculated on a regular grid through the process of propagating wavefronts, as first introduced by Vidale (1988). In Vidale's method, local planar or circular wavefronts are propagated by using a finite-difference method. Since then, several different finite-difference schemes have been developed to improve the accuracy and efficiency of the traveltime calculation (Van Trier and Symes, 1991; Podvin and Lecomte, 1991). In this chapter I present another improved finite-difference method for propagating wavefronts. The method can calculate the traveltime field in a model of large velocity contrasts and the geometrical amplitude field in regions where the wave field is regular. The implementation of the method is fully vectorizable. The results of the computation are sufficiently accurate for imaging seismic reflection data.

I begin this chapter by reviewing some well-known results of zero-order asymptotic ray theory that are relevant to the calculation of traveltimes and geometrical amplitudes of seismic waves. I also derive two new partial differential equations for the amplitude calculation. Then I approximate partial differential equations by finite differences in polar coordinates and solve them through the process of wavefront propagation. The scheme for calculating traveltimes and geometrical amplitudes is described in detail. Initial and boundary conditions are also addressed. After that, I demonstrate the computation with several synthetic examples. Finally, I summarize the results of this chapter and discuss some limitations of the method.

Zeroth-order asymptotic ray theory

The scalar wave equation for a 2-dimensional, isotropic medium of constant density has a well-known form:

$$\frac{\partial^2 P}{\partial x^2} + \frac{\partial^2 P}{\partial z^2} = \frac{1}{v^2}\frac{\partial^2 P}{\partial t^2}, \tag{1}$$

where $P = P(t, x, z)$ is a scalar field, and $v = v(x, z)$ is the velocity field of the medium.

Using asymptotic ray theory, one can expand the trial solution of the wave equation into a ray series at the infinite frequency (Červený et al., 1977). By taking the leading term of this ray series, one can construct an approximate Green's function for Kirchhoff depth migration as follows:

$$G(\omega, x, z; x_s) = A(x, z; x_s) e^{i\omega\tau(x,z;x_s)}. \tag{2}$$

where $\tau(x, z; x_s)$ is the traveltime it takes for a wave to propagate from a source point x_s on the surface to a subsurface point (x, z), $A(x, z; x_s)$ describes the amplitude decay of this propagation caused by geometrical wavefront spreading. The traveltime field satisfies the eikonal equation that relates the gradient of the traveltime field to the velocity model as follows:

$$|\nabla\tau|^2 = \frac{1}{v^2}. \tag{3}$$

The geometrical amplitude field honors the zeroth-order transport equation:

$$\nabla\tau \cdot \nabla A + \frac{1}{2}(\nabla^2\tau)A = 0, \tag{4}$$

where $\cdot$ stands for the dot product of two vectors. The approximate Green's function in equation (2) is good up to the point that the velocities of the given model change by a large fraction of themselves within a wavelength of seismic waves.

The traveltime field

Traditionally, the eikonal equation is solved by using the method of characteristics (Červený et al., 1977; Nolet, 1987). The characteristic curves of this equation are rays described by the system of ray equations, as follows:

$$\left\{ \begin{array}{lllllll} \frac{dx}{ds} & = & v\tau_x & \qquad & \frac{d\tau_x}{ds} & = & -\frac{v_x}{v^2} \\ \\ \frac{dz}{ds} & = & v\tau_z & \qquad & \frac{d\tau_z}{ds} & = & -\frac{v_z}{v^2}, \end{array} \right. \tag{5}$$

where variable s is the arclength along a ray, and subscripts x and z denote partial derivatives with respect to x and z, respectively. The system of ray equations are ordinary differential equations (ODE), and thus can be solved by a numerical integration method, such as a high-order Runge-Kutta method (Press et al., 1986). The solutions to these equations define a transformation between Cartesian coordinates (x, z) and ray coordinates (s, γ) as follows:

$$\left\{ \begin{array}{lll} x & = & x(s, \gamma) \\ \\ z & = & z(s, \gamma), \end{array} \right. \tag{6}$$

where γ is a variable determined by initial conditions. For a point source, γ is usually chosen to be the take-off angle of a ray. For each fixed γ, equation (6) gives the Cartesian coordinates of a ray as a function of s. The domain of γ spans a fan of rays covering the whole (x, z) space. Substituting (x, z) in equation (6) into the eikonal equation yields an ODE along each ray:

$$\frac{d\tau}{ds} = \frac{1}{v}. \tag{7}$$

The solution to this ODE is simply an integral along the ray:

$$\tau(x(s,\gamma), z(s,\gamma)) = \tau_0 + \int_{s_0}^{s} \frac{d\xi}{v(x(\xi,\gamma), z(\xi,\gamma))}, \tag{8}$$

where τ_0 is the initial traveltime at the source location. This method of traveltime calculation is called the ray-tracing method. The ray tracing method computes the traveltimes along rays that generally have irregular geometries, producing traveltime fields on an irregular grid in Cartesian coordinates.

Many seismic modeling and imaging algorithms need traveltime fields on a regular Cartesian grid. An efficient way to obtain such traveltime fields is to solve the eikonal equation directly in Cartesian coordinates using a finite-difference scheme. The finite-difference calculation of traveltimes can be interpreted as a wavefront-propagation process in which the wavefronts are locally propagated from grid points where traveltimes are known to neighboring grid points where traveltimes are unknown. This process starts in the vicinity of the source position where the traveltimes are computed by assuming a local constant velocity, and proceeds on an expanding computational front until all grid points are filled. The gradient field of traveltime can also be computed through wavefront propagation. The gradient field is a vector field, and thus has two components in two dimensions. In order to determine both components, one more equation is needed besides the eikonal equation. Van Trier and Symes (1990) assumed a continuous gradient field and used the following simple relation:

$$\frac{\partial \tau_z}{\partial x} = \frac{\partial \tau_x}{\partial z}, \tag{9}$$

where τ_x and τ_z are the two components of the traveltime gradient. Once the gradient field is computed, its integration gives the traveltime field.

The geometrical amplitude field

If I assume that the traveltime field has been computed by solving the eikonal equation, then the zeroth-order transport equation becomes a first-order, linear, partial differential equation, and can be solved, in principle, by a finite-difference method. An easier approach is to solve the transport equation in ray coordinates (Červený et al., 1977), and transform the analytical solution to Cartesian coordinates, which yields

$$A(x,z;x_s) = R(\gamma)\sqrt{\frac{v_0}{|J(x,z;x_s)|v(x,z)}}, \tag{10}$$

where R is the radiation pattern of the source, $\gamma = \gamma(x,z;x_s)$ is the take-off angle of the ray that starts at the surface point x_s and reaches subsurface point (x,z), v_0 is the velocity at the source position, and $J(x,z;x_s)$ is the geometrical spreading factor. For a 2-D medium and a line source, the geometrical spreading factor is equal to the absolute value of the Jacobian of the transformation from Cartesian coordinates to ray coordinates, as follows:

$$J(x, z; x_s) = \frac{\partial(x, z)}{\partial(s, \gamma)}. \tag{11}$$

It can be shown that

$$\left(\frac{\partial \gamma}{\partial x}\right)^2 + \left(\frac{\partial \gamma}{\partial z}\right)^2 = \frac{1}{|J(x, z)|^2}. \tag{12}$$

This equation has a form similar to the eikonal equation, and it defines a relation between γ and $|J|$. If the gradient field of γ is known, then rearranging equation (12) yields a formula for calculating $|J|$.

The field source is often well approximated by a point source. Červený and Hron (1980) found that in such a situation, the geometrical spreading factor $|J|$ for a line source should be multiplied by a factor η to take account of the geometrical spreading in the third dimension on which the velocity field does not depend. He showed that

$$\eta(x(s, \gamma), z(s, \gamma); x_s) = \frac{1}{v_0} \int_0^s v(x(\xi, \gamma), z(\xi, \gamma)) d\xi. \tag{13}$$

Clearly, the calculation of the amplitude field is subject to the calculation of γ, the gradient of γ and η.

Two new partial differential equations

Conventionally, γ and η are calculated through kinematic ray-tracing, and $|J|$ is calculated through dynamic ray-tracing. However, as with the traveltime calculation by ray-tracing, the results of these calculations are given along rays and have to be interpolated onto a Cartesian grid, which may be difficult. Vidale and Houston (1990) developed a method in which the γ field for a given source point is estimated from the traveltime fields associated with four neighboring source points. The method uses the first-order finite-differences to approximate the gradient field of γ, and computes the geometrical spreading factor for a line source using equation (12). Their method produces accurate geometrical amplitude field in the case of a smoothly varying velocity structure.

Here I present a new approach. I compute the γ and η fields by solving two partial differential equations which I derive in Appendix **??**. To compute the γ field and its gradient, I solve the partial differential equation:

$$\frac{\partial \tau}{\partial x}\frac{\partial \gamma}{\partial x} + \frac{\partial \tau}{\partial z}\frac{\partial \gamma}{\partial z} = 0 \tag{14}$$

with the initial condition that in the vicinity of the source point x_s, $\gamma(x, z; x_s)$ is equal to the take-off angle computed by assuming a local constant velocity. Similarly, I compute $\eta(x, z; x_s)$ by solving the partial differential equation:

$$\frac{\partial \tau}{\partial x}\frac{\partial \eta}{\partial x} + \frac{\partial \tau}{\partial z}\frac{\partial \eta}{\partial z} = \frac{1}{v_0}. \tag{15}$$

The computation is initiated in the vicinity of the source point where $\eta(x, z)$ is computed by equation (13) with the constant velocity assumption. It should be noted that equations (14) and (15) are valid only in regions where the wave field is regular. In the next section, I describe the numerical algorithms for solving equations (3), (14) and (15).

The finite-difference scheme with an adaptive step-size

Stability, accuracy, and efficiency are three requirements of utmost concern for a finite-difference algorithm. To achieve high efficiency, I choose to conduct the computations in polar coordinates and design a first-order finite-difference scheme whose implementation is fully vectorizable along the circular computational front at each step of wavefront propagation. Using polar coordinates also reduces the cases for which backward propagation has to be performed. Stability of the algorithm is ensured by adapting the step-size of the wavefront propagation to the directions of local plane waves. Because the method uses a first-order finite-difference approximation, its accuracy of is comparable to other first-order finite-difference methods.

The representation of a velocity field

For a given source location, an input velocity field is mapped onto a regular grid in polar coordinates whose origin is located at the source point, as shown in Figure 1. The grid divides the space into cells. In order to describe properly the wave propagation in these cells, it is necessary to determine the velocity representation within each cell. Like Podvin and Lecomte (1991), I use constant velocity cells. I assume that the grid sizes are small so that each individual cell can be treated as a small rectangle of dimensions Δr by $r\Delta\theta$, as shown in Figure 2. At the boundaries of cells, the velocity field is generally discontinuous. The interfaces of the velocity field are formed along the boundaries of cells. As will be seen later in examples, this approximation is generally adequate for the traveltime calculation. But it may become inadequate for the amplitude calculation unless the velocity field varies smoothly.

The computations of the traveltime field and its gradient

The traveltime field and its gradient can be calculated through the process of wavefront propagation. With the assumption that the actual wavefront is locally well approximated by a plane, I compute the gradient components of the traveltime field by first-order finite differences and propagate them using Snell's law. The traveltime field is obtained by integrating the gradient field during the propagation process. Because the finite-difference approximation to the traveltime gradient calculation requires that the traveltime field is continuous and because first arrivals always have continuous traveltime field, my algorithm, like other finite-difference algorithms, ex-

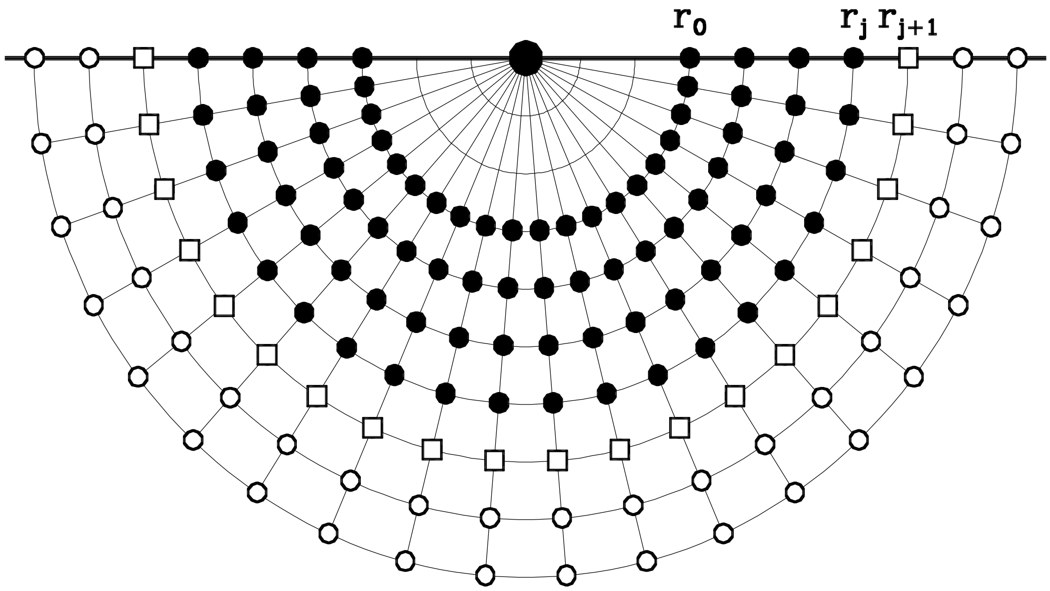

Figure 1: A regular grid in polar coordinates whose origin is at the given source point, as indicated by the large black dot. The small black dots indicate the grid points where the traveltimes are known, and the small squares indicate the grid points at which the traveltimes are to be calculated in the next step of wavefront propagation. findif2-vppolar [ER]

plicitly calculates the traveltimes of the first arrivals by selecting minimum traveltimes at each step of wavefront propagation.

The eikonal equation in polar coordinates is as follows:

$$\left(\frac{\partial \tau}{\partial r}\right)^2 + \frac{1}{r^2}\left(\frac{\partial \tau}{\partial \theta}\right)^2 = \frac{1}{v^2(\theta, r)}. \tag{16}$$

To have a discrete representation of this equation, I sample the traveltime field on the grid points and the gradient field at the centers of cell boundaries. Let i be the index of the angle sampling and j be the index of the radius sampling. As shown in Figure 2, $\tau_{i,j}$ denotes the traveltime at grid point (i,j), $u_{i,j}$ denotes the component of the gradient field tangential to the constant radius boundary between grid points (i,j) and $(i+1,j)$, and $\hat{w}_{i,j}$ denotes the component of the gradient field tangential to the constant angle boundary between grid points (i,j) and $(i,j+1)$.

The propagation process starts from the vicinity of the source point where the velocity field is assumed to be constant. As shown in Figure 1, r_0 is the radius of a circle centered at the source point, within which the velocity is v_0; then

$$\tau_{i,j} = \frac{j\Delta r}{v_0} \qquad \text{for} \quad j\Delta r \leq r_0.$$

Starting from this circle, the local plane wavefronts are propagated by following the expansion of the circle. Suppose that the computation has proceeded to the circle of radius r_j and that $\tau_{i,j}$ are known for all i. In the next step of wavefront propagation,

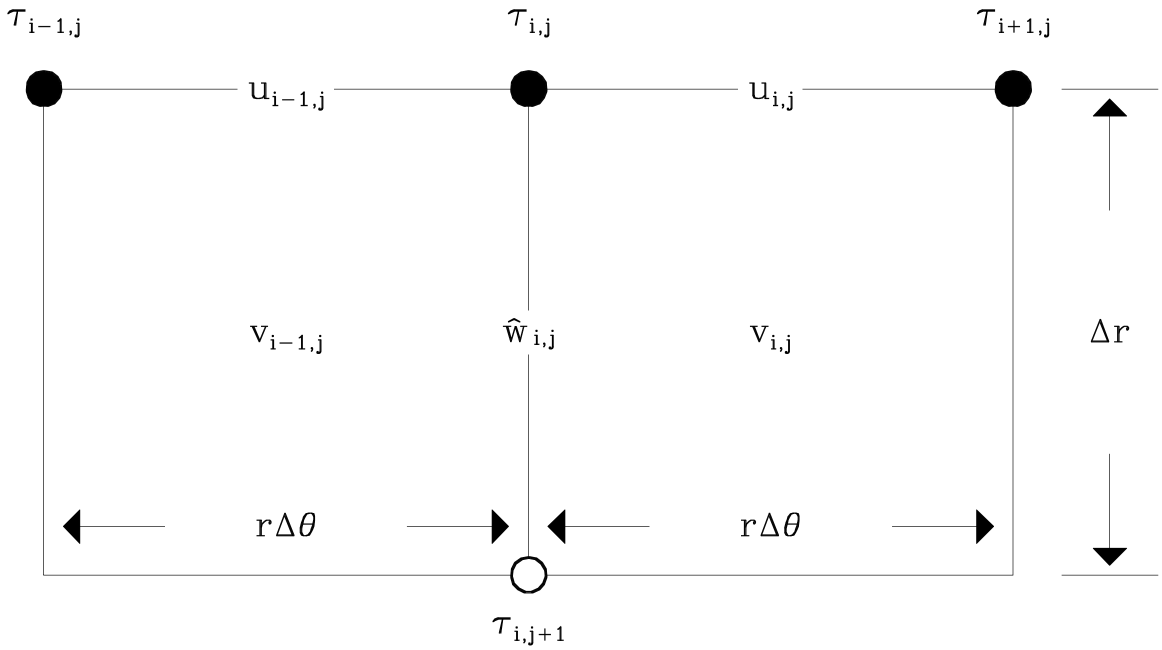

Figure 2: The grid and notations for traveltime calculation. Because Δr and $\Delta\theta$ are very small, a cell in the polar grid is approximated by a rectangular cell of size Δr by $r\Delta\theta$. findif2-vpgrid1 [ER]

the traveltimes at all grid points along the circle of radius r_{j+1} are to be calculated With the approximation of local plane waves,

$$u_{i,j} = \frac{1}{r_j}\frac{\partial \tau}{\partial \theta} = \frac{\tau_{i+1,j} - \tau_{i,j}}{r_j \Delta\theta}. \tag{17}$$

According to Snell's law, $u_{i,j}$ is continuous across the constant-radius boundary between grid point (i,j) and $(i+1,j)$ until the critical angle is reached. Beyond the critical angle, the wave propagates along the boundary with velocity $v_{i,j}$. Therefore, after crossing the boundary,

$$u_{i,j} = \min(u_{i,j}, v_{i,j}^{-1}). \tag{18}$$

Let $w_{i,j}$ be the component of the traveltime gradient orthogonal to the boundary. After crossing the boundary, $w_{i,j}$ can be computed from the eikonal equation.

$$w_{i,j} = \frac{\partial \tau}{\partial r} = \sqrt{v_{i,j}^{-2} - u_{i,j}^2}. \tag{19}$$

Two components $u_{i,j}$ and $w_{i,j}$ of the traveltime gradient determine the propagation direction of the local plane wave in the cell with velocity $v_{i,j}$. Similarly, $\hat{w}_{i,j}$ is continuous across the constant-angle boundary between (i,j) and $(i,j+1)$. By propagating $w_{i,j}$, I compute $\hat{w}_{i,j}$ in four different cases as follows:

1. $u_{i-1,j} \geq 0$ and $u_{i,j} \leq 0$

$$\hat{w}_{i,j} = \min(w_{i-1,j}, w_{i,j}, v_{i-1,j}^{-1}, v_{i,j}^{-1})$$

2. $u_{i-1,j} \geq 0$ and $u_{i,j} > 0$

$$\hat{w}_{i,j} = \min(w_{i-1,j}, v_{i,j}^{-1})$$

3. $u_{i-1,j} < 0$ and $u_{i,j} \leq 0$

$$\hat{w}_{i,j} = \min(w_{i,j}, v_{i-1,j}^{-1})$$

4. $u_{i-1,j} < 0$ and $u_{i,j} > 0$

$$\hat{w}_{i,j} = \min(v_{i-1,j}^{-1}, v_{i,j}^{-1}).$$

This scheme is equivalent to the one described by Podvin and Lecomte (1991). Here I give a brief explanation. For convenience, I refer to the wavefront confined between grid points $(i-1, j)$ and (i, j) as wavefront i, the boundary between grid points (i, j) and $(i, j+1)$ as boundary i, and the cell with velocity $v_{i,j}$ as medium i. The explanations of these four cases are as follows:

1. Both wavefronts $(i-1)$ and i propagate towards boundary i. Because of the plane wave assumption, $\hat{w}_{i,j}$ can be equal to either $w_{i-1,j}$ or $w_{i,j}$. These two plane waves may be refracted at boundary i. If $w_{i-1,j} > v_{i,j}^{-1}$, then a refracted wave propagates along the boundary with velocity $v_{i,j}$. If $w_{i,j} > v_{i-1,j}^{-1}$, then a refracted wave propagates along the boundary with velocity $v_{i-1,j}$. To obtain the minimum traveltime at grid point $(i, j+1)$, $\hat{w}_{i,j}$ is set to the minimum of the four possible values.

2. Only wavefront $(i-1)$ propagates towards boundary i. When $w_{i-1,j} > v_{i,j}^{-1}$, the refraction occurs along the boundary on the side of medium i. Thus, $\hat{w}_{i,j}$ takes the minimum of $w_{i-1,j}$ and $v_{i,j}^{-1}$ in order to obtain the minimum $\tau_{i,j+1}$.

3. Only wavefront i propagates towards boundary i. When $w_{i,j} > v_{i-1,j}^{-1}$, the refraction occurs along the boundary on the side of medium $(i-1)$. Thus, $\hat{w}_{i,j}$ takes the minimum of $w_{i,j}$ and $v_{i-1,j}^{-1}$ in order to obtain the minimum $\tau_{i,j+1}$.

4. Both wavefronts $(i-1)$ and i propagate away from boundary i. The diffracted waves propagate along the boundary with velocities $v_{i-1,j}$ and $v_{i,j}$. To obtain the minimum $\tau_{i,j+1}$, $\hat{w}_{i,j}$ takes the minimum of $v_{i-1,j}$ and $v_{i,j}$.

Because traveltime increases monotonically as wavefronts propagate, selecting local minimum traveltimes at each step of wavefront propagation will produce global minimum traveltime at each grid point.

The two side-boundaries are treated as follows:

For $i = 1$,

$$\hat{w}_{1,j} = \begin{cases} w_{1,j} & \text{if} \quad u_{1,j} \leq 0 \\ v_{1,j}^{-1} & \text{otherwise.} \end{cases}$$

For $i = n$,

$$\hat{w}_{n,j} = \begin{cases} w_{n,j} & \text{if} \quad u_{n,j} \le 0 \\ v_{n,j}^{-1} & \text{otherwise,} \end{cases}$$

These side-boundary conditions ensure no wavefront propagates into the medium from the two side-boundary.

To maintain the stability of the computation, it is required that the wavefront propagation process respect the causality condition (Vidale, 1988; Podvin and Lecomte, 1991). This causality condition is equivalent to the Courant condition in numerical calculus (Press et al., 1986), and can be expressed as the following inequality:

$$w_{i,j} > \frac{\Delta r}{v_{i,j}\sqrt{\Delta r^2 + (r_j \Delta\theta)^2}}. \tag{20}$$

If the step-size of the propagation is adapted to the propagation directions of local plane waves as follows:

$$\Delta r = \min_i \left[r_j \Delta\theta \frac{|w_{i,j}|}{|u_{i,j}|} \right], \tag{21}$$

then the inequality in equation (20) is satisfied for all i.

After $\hat{w}_{i,j}$ for all i are known, the traveltimes can be computed by simple integration:

$$\tau_{i,j+1} = \tau_{i,j} + \hat{w}_{i,j}\Delta r \qquad \text{for all } i, \tag{22}$$

which completes one step of the propagation. These procedures are repeated until all grid points are covered. The implementation of this algorithm is quite simple and the program is fully vectorizable along index i (Zhang, 1991).

One problem not yet addressed is the possibility of refractions along the constant-radius boundaries, which may initiate wave propagations toward the source. To make the algorithm more complete, I handle such situations by using Podvin and Lecomte's method in polar coordinates and performing backward extrapolation as necessary. After obtaining the traveltimes in polar coordinates, I map them to Cartesian coordinates.

The computation of the amplitude field

To compute the geometrical amplitudes, equations (14) and (15) need to be solved. In polar coordinates, these two equations become

$$\frac{\partial\tau}{\partial r}\frac{\partial\gamma}{\partial r} + \frac{1}{r^2}\frac{\partial\tau}{\partial\theta}\frac{\partial\gamma}{\partial\theta} = 0 \tag{23}$$

and

$$\frac{\partial \tau}{\partial r}\frac{\partial \eta}{\partial r} + \frac{1}{r^2}\frac{\partial \tau}{\partial \theta}\frac{\partial \eta}{\partial \theta} = \frac{1}{v_0}, \tag{24}$$

respectively. After the traveltime field has been computed, these two equations become first-order, linear, partial differential equations for γ and η. The algorithms for solving these two equations are similar to the one for solving the eikonal equation.

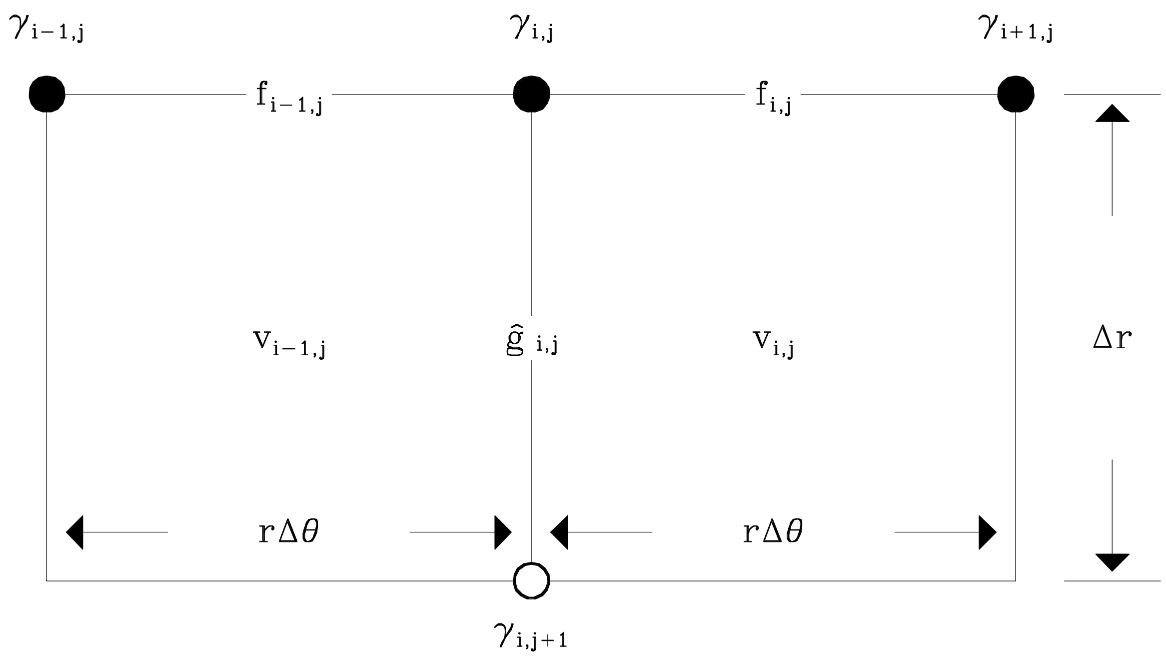

Figure 3: The grid and notations for amplitude calculation. Because Δr and $\Delta\theta$ are very small, a cell in the polar grid are approximated by a rectangular cell of size $\Delta r \times r\Delta\theta$. findif2-vpgrid2 [ER]

To solve equation (23), the initial condition is set in the vicinity of the source as follows:

$$\gamma_{i,j} = \theta_0 + i\Delta\theta \qquad \text{for} \qquad j\Delta r \le r_0. \tag{25}$$

where θ_0 is the initial angle of the polar coordinates. The component of the gradient field of γ tangential to the constant-radius boundary is computed with finite difference approximations.

$$f_{i,j} = \frac{1}{r_j}\frac{\partial \gamma}{\partial \theta} = \begin{cases} \dfrac{\gamma_{i+1,j} - \gamma_{i,j}}{r_j \Delta\theta} & \text{if} \quad w_{i,j} \neq 0. \\ 0. & \text{otherwise.} \end{cases} \tag{26}$$

From equation (23),

$$g_{i,j} = \frac{\partial \gamma}{\partial r} = \begin{cases} -\dfrac{u_{i,j}}{w_{i,j}} f_{i,j} & \text{if} \quad w_{i,j} \neq 0. \\ \\ 0. & \text{otherwise.} \end{cases} \tag{27}$$

Let $\hat{g}_{i,j}$ denote the component of the gradient field of γ tangential to the constant angle boundary, as shown in Figure 3. As with the calculation of $\hat{w}_{i,j}$, the calculation of $\hat{g}_{i,j}$ also involves four different cases:

1. $u_{i-1,j} \geq 0$ and $u_{i,j} \leq 0$

$$\hat{g}_{i,j} = \begin{cases} g_{i-1,j} & \text{if } \hat{w}_{i,j} = w_{i-1,j} \\ \\ g_{i,j} & \text{if } \hat{w}_{i,j} = w_{i,j} \\ \\ 0 & \text{if } \hat{w}_{i,j} = v^{-1}_{i-1,j} \text{ or } v^{-1}_{i,j} \end{cases}$$

2. $u_{i-1,j} \geq 0$ and $u_{i,j} > 0$

$$\hat{g}_{i,j} = \begin{cases} g_{i-1,j} & \text{if } \hat{w}_{i,j} = w_{i-1,j} \\ \\ 0 & \text{if } \hat{w}_{i,j} = v^{-1}_{i,j} \end{cases}$$

3. $u_{i-1,j} < 0$ and $u_{i,j} \leq 0$

$$\hat{g}_{i,j} = \begin{cases} g_{i,j} & \text{if } \hat{w}_{i,j} = w_{i,j} \\ \\ 0 & \text{if } \hat{w}_{i,j} = v^{-1}_{i-1,j} \end{cases}$$

4. $u_{i-1,j} < 0$ and $u_{i,j} > 0$

$$\hat{g}_{i,j} = 0$$

If $\hat{w}_{i,j}$ and $\hat{g}_{i,j}$ are calculated in one subroutine, then the implementation is simple and the program is fully vectorizable along index i. The integration of $\hat{g}_{i,j}$ yields

$$\gamma_{i,j+1} = \gamma_{i,j} + \hat{g}_{i,j} \Delta r. \tag{28}$$

To solve equation (24), I rewrite it as follows:

$$\eta_r = \frac{1}{\tau_r}[\frac{1}{v_0} - \frac{1}{r^2}\tau_\theta \eta_\theta].$$

Referring to the algorithm for calculating $\tau(r, \theta)$ and $\gamma(r, \theta)$, one can easily construct the algorithm for calculating $\eta(r, \theta)$.

The geometrical spreading factor can be determined in polar coordinates from equation (12) as follows:

$$|J(r_j, \theta_i)| = \frac{1}{\sqrt{\left(\frac{\partial \gamma}{\partial r}\right)^2 + \left(\frac{1}{r_j}\frac{\partial \gamma}{\partial \theta}\right)^2}} = \frac{1}{\sqrt{f_{i,j}^2 + g_{i,j}^2}}. \tag{29}$$

I map the results of the calculation to Cartesian coordinates and use equation (10) to calculate the geometrical amplitudes. It should be noted that equation (10) gives infinite amplitudes at caustics where the geometrical spreading factor is equal to zero. This problem comes from the fact that the zeroth-order transport equation does not properly describe the amplitudes of a scalar wave field at caustics. Although more accurate methods exist, I handle such situations by simply setting a minimum geometrical spreading factor.

Examples

Figures 4 and 5 show the results of the traveltime and amplitude calculations for a medium in which velocity increases linearly from 2 km/s at the surface to 4 km/s at the depth of 2 km. In the calculations, the sampling intervals in radius are 14 meters and in angle are 0.45 degree. The top panel of Figure 4 shows the contour lines of the traveltime field, plotted on the top of the velocity displays. The contour lines of the traveltime field display the trajectories of the wavefronts. Because of the increase in velocity with depth, the wavefronts are stretched downward. Since the analytical solution of the traveltime field is known for such a linearly increasing velocity field, it is used to check the accuracy of the computation. The bottom panel of Figure 4 shows the differences between the analytical solution and the traveltime field calculated by the finite-difference method. The differences are less than 1. ms, which is accurate enough for Kirchhoff depth migration of seismic reflection data recorded at the earth's surface. As described earlier in this chapter, the take-off angle field is related to the amplitude calculation. The top panel of Figure 5 shows the contour lines of the take-off angle field calculated by the finite-difference method. Because each ray has a unique take-off angle, the contour lines of the take-off angle field show the trajectories of the rays. As expected, rays are overturned. The bottom panel of Figure 5 shows the error distribution in the calculation of the take-off angle field. The maximum error is 0.36 degree.

For traveltime calculation, the algorithm can handle virtually arbitrary velocity models. The second example illustrates the traveltime calculation for a model containing a low velocity anomaly of square shape. The ratio of the velocities of the anomaly and the background is 1 to 3. The result of the calculation is shown in Figure 6. The circular wavefront generated by a point source located at the upper right corner of the model is greatly distorted after passing through the anomaly. The portions of the wavefront that correspond to refracted waves can be identified. The looping contour lines within the anomaly are caused by the finite grid sizes. In the lower right part of the anomaly, the first arrivals propagate back toward the source. The traveltimes in this region are calculated by backward propagations. Figure 7 compares the wave field simulated by wave-equation modeling with the traveltime field calculated by the finite-difference method. The figure displays the snapshots of the wave field at four time instants. Because a minimum phase wavelet is used in the wave-equation modeling, the contour lines of the traveltime field closely follow the first breaks of the wavelets of the first arrivals in the corresponding snapshots of the wave fields. The algorithm is not capable of calculating the amplitudes for this model because of large velocity contrasts.

The final example shows the traveltime calculation for a structure model estimated from field data. Figure 8 shows the contour lines of the traveltime field plotted on the top of the velocity field. The accuracy of the calculation is verified by comparing the result of the traveltime calculation with a high-order finite-difference solution to the scaler wave equation. A snapshot of the wave field at 1.0 second is overlain with the 1.0 second contour line of the traveltime field. The contour follows the first arrivals precisely.

Summary

By propagating the wavefronts with the finite-difference method, the traveltimes and geometrical amplitudes of seismic waves are calculated on a regular grid. The method is efficient and stable. For the traveltime calculation, the method performs well for general velocity models, but the amplitude calculation is limited to smoothly varying velocity models. This limitation results from the fact that the amplitude calculation relies on accurate traveltime gradients. The finite-difference approximation to the traveltime gradient calculation breaks down when velocity changes rapidly. Another limitation of the method is that it computes only the first-arrival field because the finite-difference approximation is valid only when the field is continuous and because a first-arrival field is always continuous. In the next chapter, I present a more accurate method for propagating wavefront, which partially overcomes these limitations.

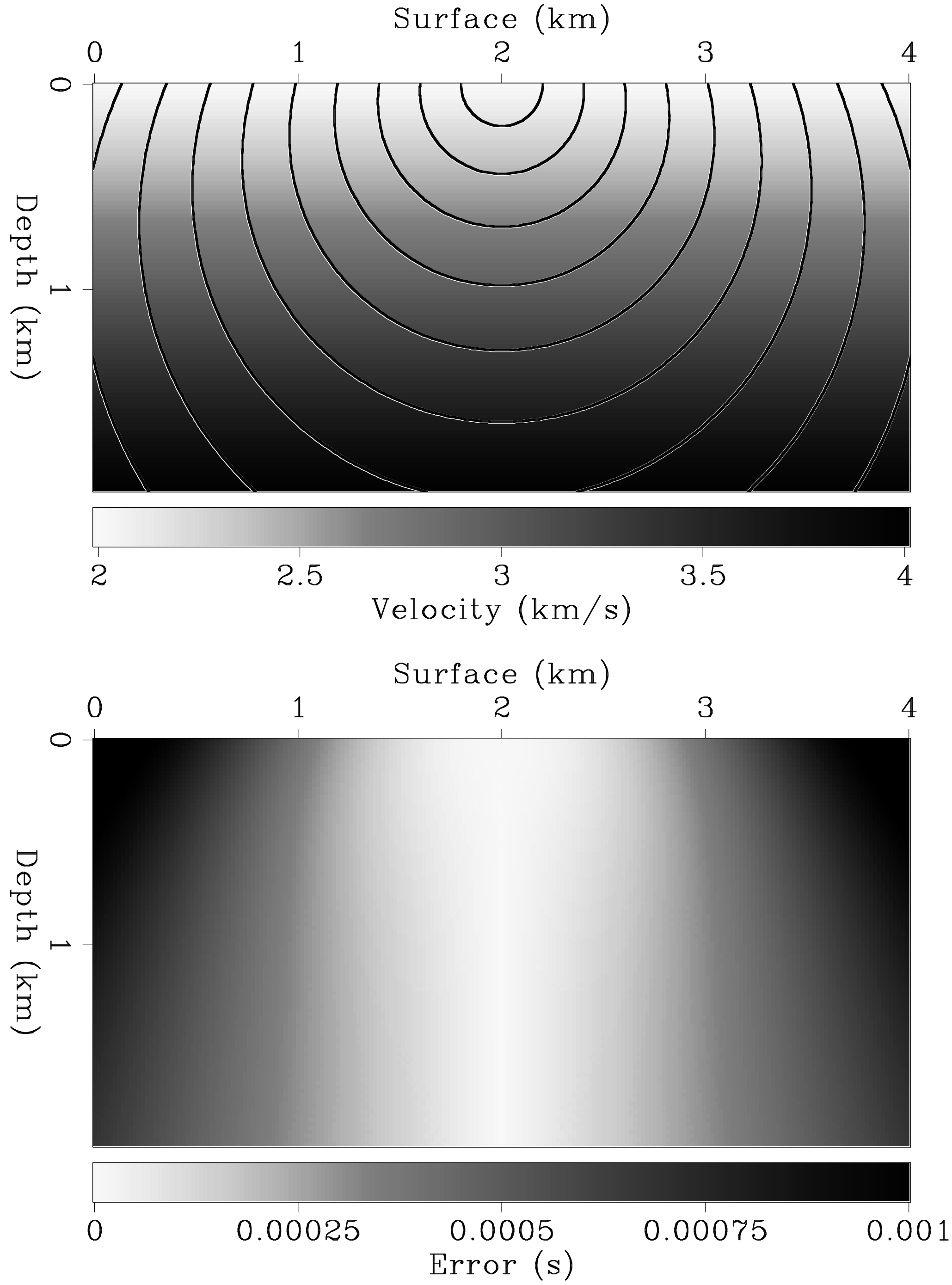

Figure 4: The traveltime calculation for a constant gradient velocity model. The background of the top panel shows the velocity field. The source is on the surface in the center of the model. Overlain on the top panel are the contour lines of the traveltime field with 0.1 second intervals. The bottom panel shows the error distribution of the calculation. findif2-ttmgra [ER]

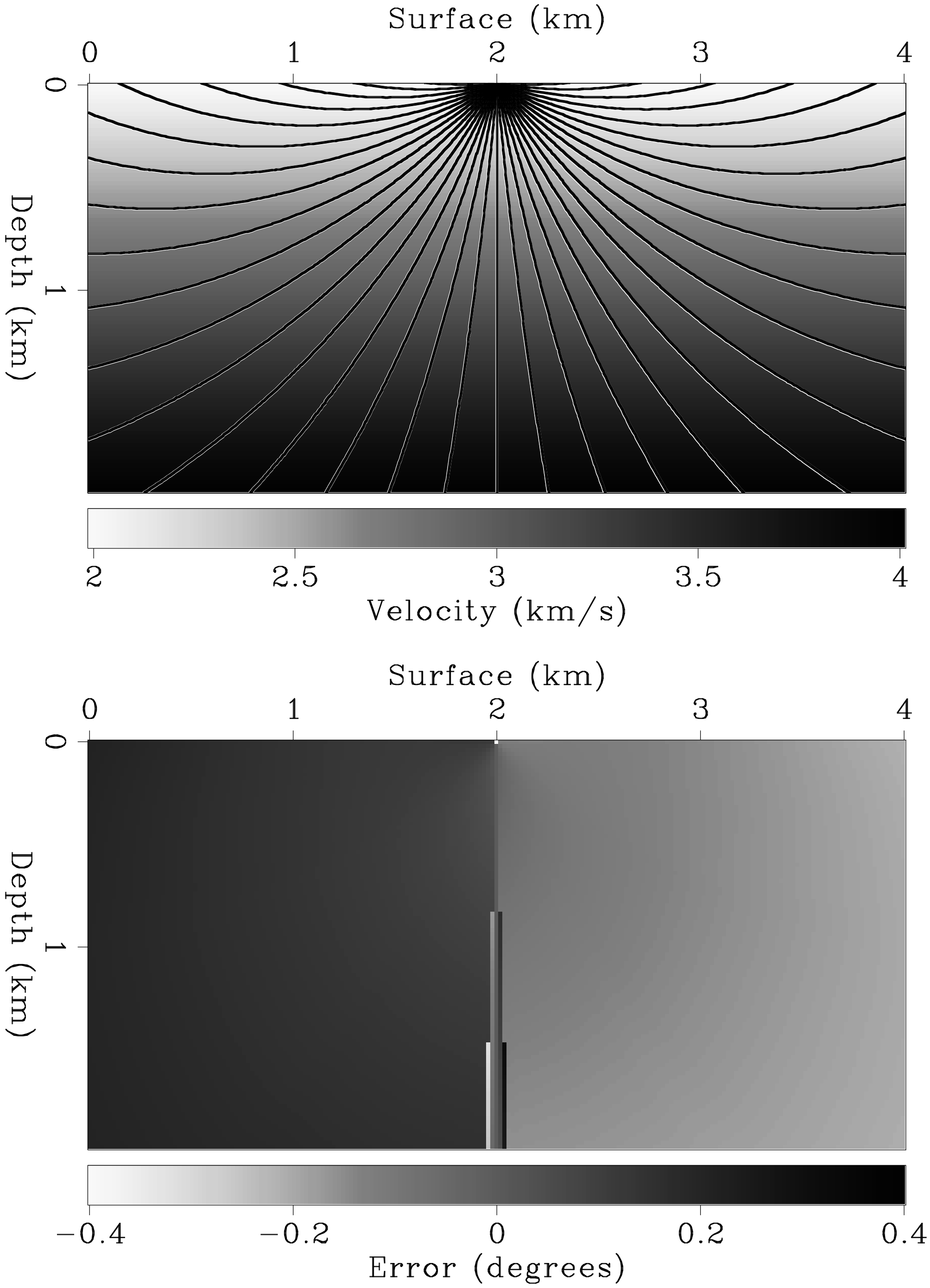

Figure 5: The take-off angle calculation for a constant gradient velocity model. The background of the top panel shows the velocity field. The source is on the surface in the center of the model. Overlain on the top panel are the contour lines of the take-off angle field with 5 degree intervals. The bottom panel shows the error distribution of the calculation. findif2-raygra [ER]

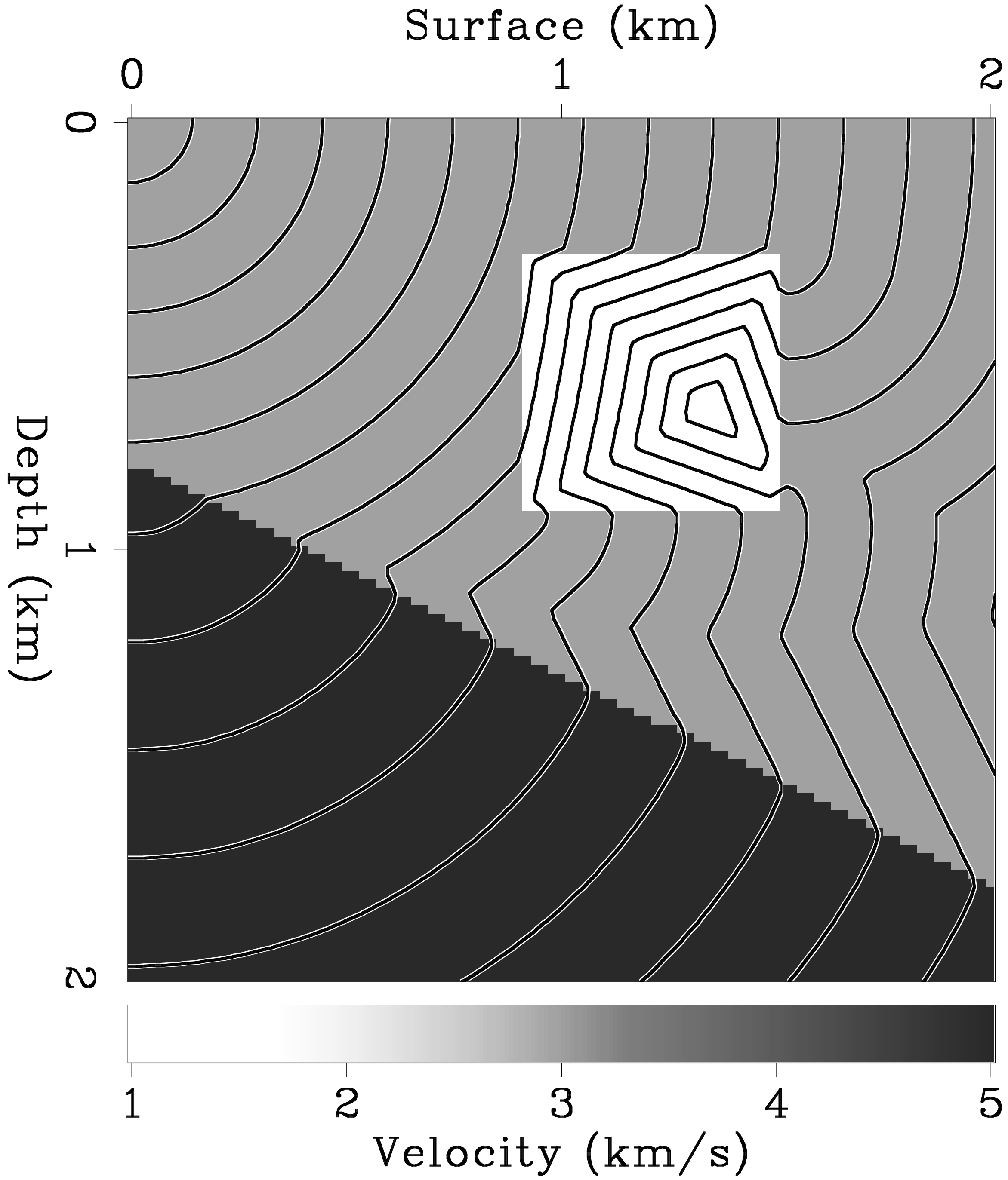

Figure 6: The traveltime calculation for a model with a sharply contrasted anomaly. The background shows the velocity field. The source is located at the upper left corner of the model. The traveltime contour lines are drawn at 0.05 second intervals. findif2-ttmrec [ER]

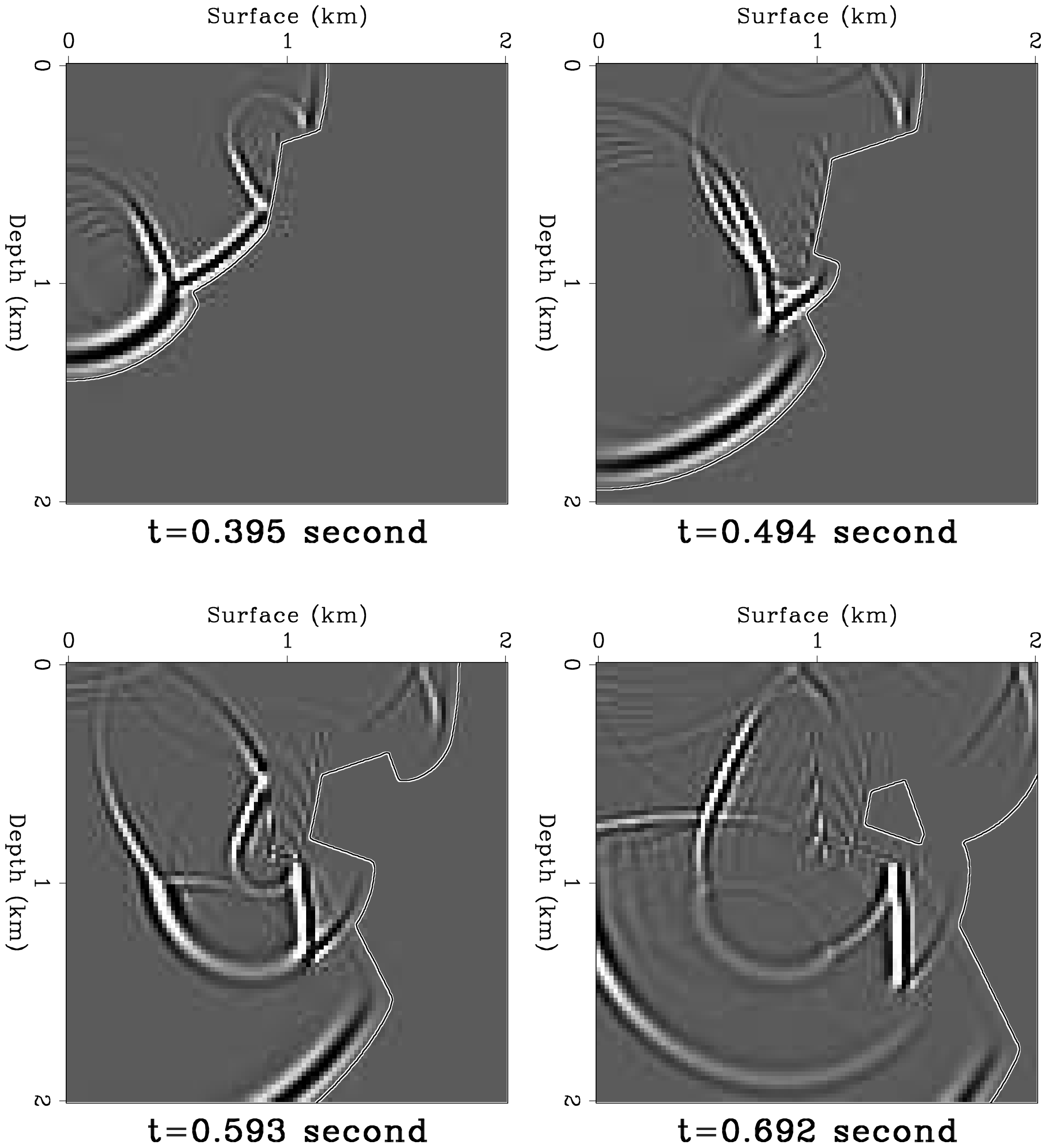

Figure 7: Comparison of the wave field simulated by wave-equation modeling with the traveltime field calculated by the finite-difference method. The intensity plots show snapshots of the wave field at four different time instants; the overlain curves are the corresponding contour lines of the traveltime field. findif2-waverec [ER]

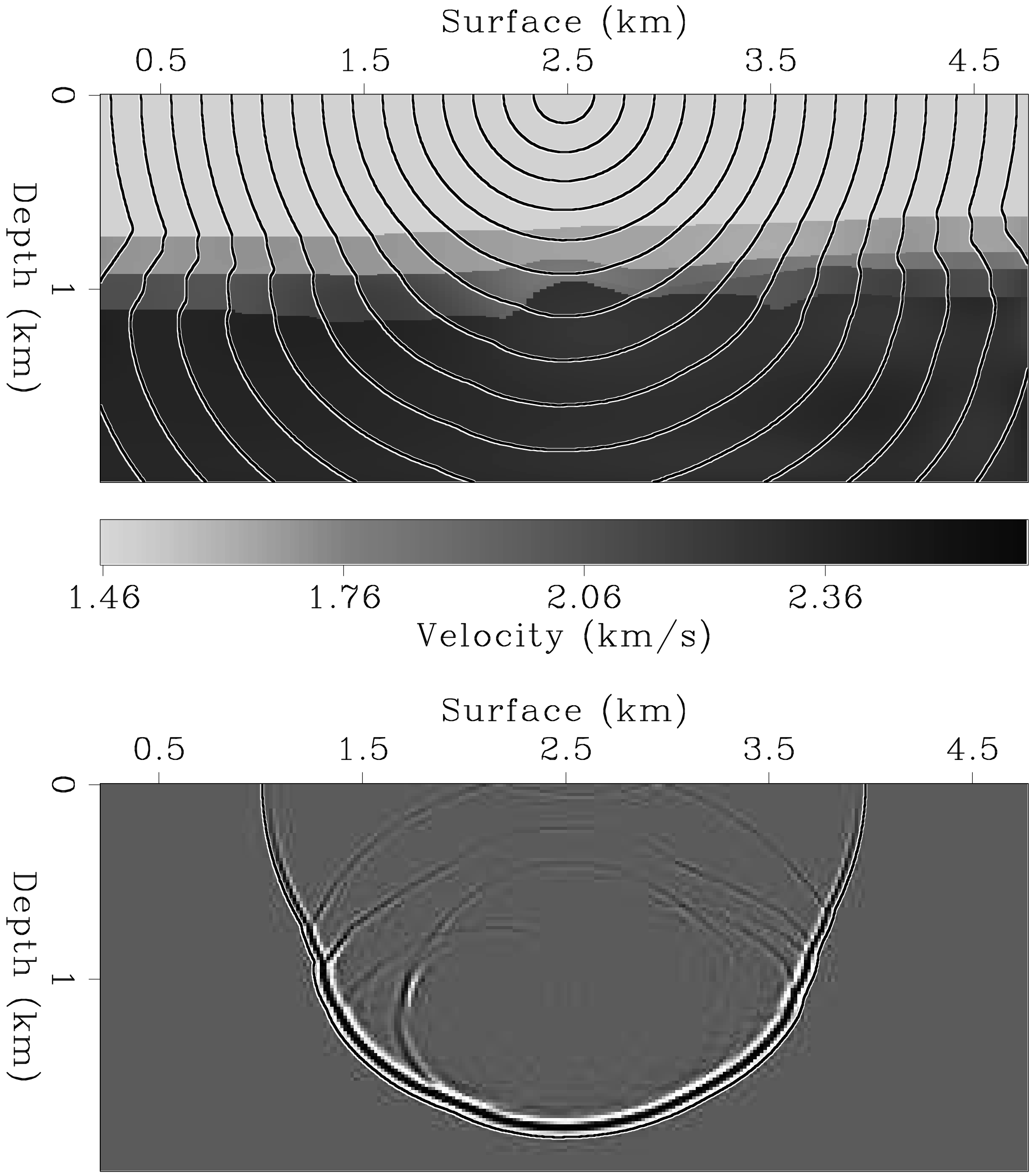

Figure 8: The traveltime calculation for a structural velocity model. The top panel displays the velocity field. Overlain are the contour lines of the traveltime field. The contour interval is 0.1 second. The bottom panel shows a snapshot of the wave field at 1.0 second, computed by wave equation modeling. The corresponding contour line of the traveltime field computed by the finite-difference method closely follows the wavefront of the first arrival. findif2-wavettmfie [ER]